es3014826

DATASET · JANUARY 2013

READS
54

5 AUTHORS, INCLUDING:

Alejandro Fernandez-Martinez
University Joseph Fourier - Grenoble 1
54 PUBLICATIONS **757** CITATIONS
SEE PROFILE

Yandi Hu
University of Houston
19 PUBLICATIONS **351** CITATIONS
SEE PROFILE

Byeongdu Lee
Argonne National Laboratory
205 PUBLICATIONS **6,479** CITATIONS
SEE PROFILE

Glenn A Waychunas
Lawrence Berkeley National Laboratory
158 PUBLICATIONS **6,839** CITATIONS
SEE PROFILE

Environmental Science & Technology

Article

pubs.acs.org/est

In Situ Determination of Interfacial Energies between Heterogeneously Nucleated $CaCO_3$ and Quartz Substrates: Thermodynamics of CO_2 Mineral Trapping

Alejandro Fernandez-Martinez,[†,∥] Yandi Hu,[‡] Byeongdu Lee,[§] Young-Shin Jun,*[,‡] and Glenn A. Waychunas[†,*]

[†]Earth Sciences Division, Lawrence Berkeley National Laboratory, One Cyclotron Road, Berkeley, California 94720, United States

[‡]Department of Energy, Environmental and Chemical Engineering, Washington University, One Brookings Drive, St. Louis, Missouri 63130, United States

[§]X-ray Science Division, Advanced Photon Source, Argonne National Laboratory, Argonne, Illinois 60439, United States

Supporting Information

ABSTRACT: The precipitation of carbonate minerals—mineral trapping—is considered one of the safest sequestration mechanisms ensuring long-term geologic storage of CO_2. However, little is known about the thermodynamic factors controlling the extent of heterogeneous nucleation at mineral surfaces exposed to the fluids in porous reservoirs. The goal of this study is to determine the thermodynamic factors controlling heterogeneous nucleation of carbonate minerals on pristine quartz (100) surfaces, which are assumed representative of sandstone reservoirs. To probe $CaCO_3$ nucleation on quartz (100) in solution and with nanoscale resolution, an in situ grazing incidence small-angle X-ray scattering technique has been utilized. With this method, a value of $\alpha' = 36 \pm 5$ mJ/m^2 for the effective interfacial free energy governing heterogeneous nucleation of $CaCO_3$ has been obtained by measuring nucleation rates at different solution supersaturations. This value is lower than the interfacial energy governing calcite homogeneous nucleation ($\alpha \approx 120$ mJ/m^2), suggesting that heterogeneous nucleation of calcium carbonate is favored on quartz (100) at ambient pressure and temperature conditions, with nucleation barriers between 2.5% and 15% lower than those expected for homogeneous nucleation. These observations yield important quantitative parameters readily usable in reactive transport models of nucleation at the reservoir scale.

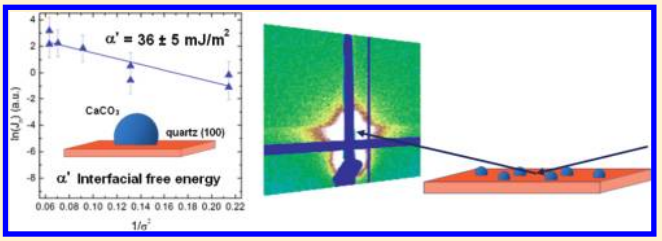

INTRODUCTION

Carbon capture and sequestration in deep geologic reservoirs such as depleted oil and gas fields, coal beds, or saline aquifers is considered to be one of the main options to mitigate the current increasing CO_2 emissions over the next century.[1] Within geologic CO_2 sequestration (GCS), stable carbonate mineral formation—mineral trapping—is one of the sequestration mechanisms that will ensure long-term storage of CO_2.[2,3] The precipitation of carbonate minerals is a widely studied chemical process due to the widespread formation of these minerals in marine and sedimentary environments,[4,5] and because of its importance in many industrial processes which include the production of construction materials, ceramics, fillers, absorbents, or the inhibition of scale formation.[6] However, the extreme physicochemical conditions present in the subsurface reservoirs targeted as potential hosts for the CO_2 make prediction of the mineralization processes difficult, especially as these are expected to occur over long time spans relative to laboratory experiments.[7]

A combination of thermodynamic and kinetic factors contributes to this uncertainty. Low supersaturations for carbonate phases are expected in GCS sites due to the relatively low solution pH values, which will be driven down upon injection of supercritical CO_2 ($scCO_2$) by formation of carbonic acid. Additionally, slow dissolution kinetics of silicate minerals, which are expected to be the main sources for cations, has been commonly hypothesized to be the limiting step for carbonation reactions.[8,9] These slow kinetics are affected by the formation of mineral coatings (e.g., amorphous silica), which in some cases act as passivating agents of the silicate mineral surface, inhibiting further dissolution.[9−11] Interestingly, some studies have pointed out that, under certain conditions, the slow precipitation kinetics of carbonate minerals can be the limiting step for the carbonation reaction.[12,13] For instance, Saldi et al. reported magnesite precipitation rates 2 to 3 orders of magnitude slower than forsterite dissolution rates.[12] Giammar et al. showed that Mg- and Si-rich carbonated

Special Issue: Carbon Sequestration

Received: April 13, 2012
Revised: May 26, 2012
Accepted: May 30, 2012
Published: May 30, 2012

solutions supersaturated with respect to magnesite can maintain the supersaturation, making the nucleation of magnesite the limiting-step for the carbonation reaction.[13] In addition, the same authors observed that magnesite seeds present in the solutions accelerated the precipitation.[13] The presence of a mineral surface is expected to lower the free energy barrier for heterogeneous nucleation if the interfacial free energy of the substrate−crystal interface is lower than that of the liquid−substrate interface.[14] In view of these results, and considering the ubiquity of mineral surfaces that could promote mineral formation in porous reservoirs, it becomes important to quantify the thermodynamic drivers for heterogeneous nucleation in order to accurately assess the extent of nucleation processes in subsurface environments.

The influence of quartz as a seed material for $CaCO_3$ precipitation has been studied previously by different authors. Lin and Singer used titration experiments at a relatively high salinity (0.1 M KCl) and observed no catalytic effect.[15] The same result was obtained by Kralj and Vdovic, who also used a high salinity solution (0.5 M NaCl).[16] A more recent study by Lioliou et al.[17] reported two different results: On one side, the presence of quartz does not influence the measured induction time with respect to the one observed for pure $CaCO_3$ saturated solutions. This suggests that heterogeneous nucleation is not taking place, and therefore it concludes that quartz does not provide a favorable surface for heterogeneous $CaCO_3$ nucleation, at least under relatively high salinity conditions. On the other hand, in another experiment in which quartz grains were added to highly saturated $CaCO_3$ solutions, these authors observed an increase of the precipitation rate. Using fits to a polynuclear growth model, the authors obtained a value for the interfacial free energy of the water−$CaCO_3$−quartz system that equals 31.1 mJ/m^2. It is worth noting that the technique used by these authors does not specifically look at the size evolution of the precipitates, but at the changes in the chemistry of the bulk fluid, and is probably unable to detect the early stages of the nucleation. In this sense, our experimental approach provides unique information by using an in situ technique that allows probing the size and the relative change of the total number of $CaCO_3$ particles nucleated under different supersaturation conditions at the nanometer scale.

Of all potential carbonate minerals, Ca^{2+}, Fe^{2+}, and Mg^{2+} carbonates are the most likely mineral phases to control carbonate concentrations in subsurface environments, due to the release of these cations upon dissolution of the silicate minerals in typical reservoir lithologies.[3] As a first step, and due to the kinetic limitations governing Mg^{2+} and Fe^{2+} carbonate formation, we have chosen to work with $CaCO_3$.[18] Also, we have performed our experiments at ambient pressure and room temperature and circum-neutral solution pH. Although these conditions are different from the high pressures and temperatures present in geologic CO_2 reservoirs, our study will provide new fundamental thermodynamic information about the nucleation processes that will still be valid under real reservoir conditions, such as the value for the interfacial free energy between the quartz substrate and the nucleated crystals. Due to the inverse solubility of carbonate minerals, the high temperature will be an additional driving force for nucleation, but it is not expected to influence the value for this interfacial free energy. Also, given the fact that the point of zero charge (pH_{PZC}) for the surface of quartz (100) is between 2 and 2.8,[19,20] and that significant surface charge does not develop on quartz until pH exceeds near-neutral values of ∼6 to 8,[19,20] we expect that the surface charge of quartz under the conditions of our experiment will be only slightly higher at the lower pH ranges predicted in geologic reservoirs, which have typical pH values of ∼3.1 upon injection of $scCO_2$, and pH values between 5.5 and 6.7 after mineral dissolution has taken place.[21]

The goal of the present study was 2-fold: (a) to develop an in situ GISAXS technique that allows determining interfacial free energies between nucleating particles and mineral substrates in an open system (i.e., keeping a constant flow of solution over the surface), and (b) to apply this technique to the study of the water−$CaCO_3$−quartz system. Our unique in situ experimental approach allowed us to gain important fundamental information about the thermodynamics of heterogeneous nucleation and opens the possibility for studying the influence that solution ionic strength, interface surface roughness and heterogeneity, and other physicochemical parameters can exert over nucleation processes in subsurface environments.

EXPERIMENTAL SECTION

In Situ Time-Resolved GISAXS Setup. The experimental setup used in this study was optimized from a similar setup developed in our group previously for in situ GISAXS batch experiments.[22,23] Mineral substrates were placed horizontally in a flow-cell designed ad hoc for the nucleation experiments. The cell internal dimensions are 10 mm × 10 mm × 15 mm. Two Kapton windows allow an X-ray beam to be directed to the substrate with an incidence angle $\alpha_i = 0.14°$, lower than the critical angle for total reflection ($\alpha_{c\text{-quartz}} \approx 0.16°$ at 12 KeV incident X-ray energy), so that the X-ray beam is reflected by the substrate. $CaCl_2$ and $NaHCO_3$ solutions were pumped from two reservoirs of 1 L each using two peristaltic pumps (model WPX1-F1/8S4−C, Welco Co. Ltd., Tokyo, Japan) at a rate of 1.6 mL/min, and mixed in a homemade mixing cell equipped with a rotating stir bar just before the solution was injected to the flow-cell. The residence time of the fluid in the cell was minimized in previous tests with colored dyes, and was estimated to be $\tau_{res} \approx 10$ s. This time is shorter than the acquisition time of GISAXS images, ensuring that the fluid supersaturation, and thus the thermodynamic driving force for nucleation, was kept constant throughout the duration of the experiment. The scattered intensity from the nucleated $CaCO_3$ particles was collected using a 2-dimensional Pilatus 2 M detector (Dectris Ltd., Baden, Switzerland) available at the beamline 12ID-B at the Advanced Photon Source (Argonne National Laboratory, USA). An incident radiation of 12 KeV X-ray energy and a sample-to-detector distance of $d_{s\text{-}d} = 2215$ mm, allowed covering a q-range of 0.005 Å^{-1} < q < 0.3 Å^{-1}.

Substrate and Solution Preparation. Quartz (100) substrates (MTI Corp., CA) were rinsed with acetone, ethanol, isopropanol, and deionized water (all chemicals were ACS reagent grade, from Sigma Aldrich), and subsequently cleaned using a mixture of Nochromix (Godax Laboratories Inc., MD) and sulfuric acid for 2 h to eliminate any organics from the substrates. They were stored in deionized water and dried with N_2 prior to the X-ray scattering experiments. The roughness of the substrates was measured using an Atomic Force Microscopy apparatus prior to the experiments, yielding R_q values $R_{q\text{-quartz}} \approx$ 1 nm. $CaCl_2$ and $NaHCO_3$ solutions of different concentrations (see Table 1A) were prepared at the APS prior to the start of the scattering experiments. The pH of the mixed solution was monitored prior to the start of every experiment, and the supersaturation was calculated using the speciation code Phreeqc Interactive (version 2.17.5, 2010)[24] and the Minteq

dx.doi.org/10.1021/es3014826 | Environ. Sci. Technol. 2013, 47, 102−109

Table 1. (A) Chemical Composition, Solution pH Value, Supersaturation with Respect to Calcite and ACC and Temperature of the Different Solutions Used in the Nucleation Experiments. (B) Measured Values for the Different Interfacial Free Energies Governing Heterogeneous Nucleation of Calcite or ACC on quartz (100). α' Values Have Been Obtained from the Linear Regression of the Measured Nucleation Rates Plotted against the Inverse of the Supersaturation σ[a]

(A)

sample	$[Ca^{2+}]$ (M)	$[HCO_3^-]$ (M)	pH	$\sigma_{calcite}$	σ_{ACC}	T (°C)
S1	0.05	0.01	7.60	3.98	−0.81	25
S2	0.05	0.007	7.61	3.78	−1.02	25
S3	0.05	0.005	7.59	3.31	−1.48	25
S4	0.01	0.004	7.85	2.76	−2.03	25
S5	0.01	0.002	7.59	2.16	−2.62	25

(B)

polymorphs	α' (mJ/m^2)	$\alpha_{water\text{-}quartz}$ (mJ/m^2)	$\alpha_{water\text{-}calcite/ACC}$ (mJ/m^2)	$\alpha_{calcite/ACC\text{-}quartz}$ (mJ/m^2)
calcite	36	360[b]	120[c]	211
ACC	27	360[b]	50[d]	328

[a] $\alpha_{calcite/ACC\text{-}quartz}$ values have been calculated using eq 4. [b] Ref 43. [c] Average $\alpha_{water\text{-}calcite}$ value from refs 36−39. [d] Estimated value for $\alpha_{water\text{-}ACC}$ under the assumption that it should be lower than the lower value reported for $\alpha_{water\text{-}calcite}$, given that the ACC structure is highly hydrated, which would tend to lower its interfacial free energy in contact with water.

database. Saturation index with respect to amorphous calcium carbonate has been calculated using the solubility constant reported by Brecevic and Nielsen (1989).[25]

Scattering Data Processing and Analysis. Images of the scattered intensity were acquired every 2 min, with a lapse time of 10 s between images. Dark current subtraction and transmission normalization were applied to all the images before data analysis. The transmission was calculated from the values of the incident and the transmitted intensity as measured using an ionization chamber and a photodiode placed on the beam stop, respectively. To isolate the scattering signal from the nucleated particles from any parasite interface scattering, the first image acquired after the substrate is completely covered by the solution has been subtracted from the rest. The scattering intensity for an isotropic system is proportional to:

$$I_{GISAXS}(q) = I(0) \times P(q, R, \sigma_d) \times S(q) \quad (1)$$

where $P(q,R,\sigma_d)$ is the form factor, $S(q)$ is the structure factor and q is the momentum transfer.[26] The average vertical and lateral particle sizes can be obtained from the distribution of the scattering intensity along the momentum transfer directions perpendicular (q_z) and parallel (q_{xy}) to the plane of the substrate, respectively. To this end, the 2-dimensional images were integrated using vertical and horizontal cuts of the intensity. The intensity in the extracted 1-dimensional curves was modeled using a log-normal polydisperse model of noninteracting spherical particles,[27] with

$$P(q, R, \sigma) = (\Delta\rho)^2 \int n(R, \sigma_d) V^2 \frac{9(\sin(qr) - qR\cos(qR))^2}{(qR)^6} dR \quad (2)$$

where $n(R,\sigma_d)$ is the log-normal distribution, which is used to represent the observed size polydispersity of the nucleated particles, with R being the mean radius of the particle and σ_d its standard deviation. V and $\Delta\rho$ are the particle volume and the electronic density difference (or contrast) between the particle and the surrounding solution. The IRENA package was used to perform fits of the experimental data.[28] The use of a spherical model for the particle shape is based upon the observation of isotropic scattering in the 2-dimensional images. Nonspherical shapes would yield different distributions of the scattering radiation.[26]

Classical Nucleation Theory. Two main parameters control the height of the thermodynamic barrier for nucleation of a new phase from a saturated solution: the interfacial free energy, α', and the supersaturation, σ.[14] The supersaturation is defined as $\sigma = \ln\{(Ca^{2+})(CO_3^{2-})/K_{sp}\}$, where the terms in the parentheses denote the activity of Ca^{2+} and CO_3^{2-}, respectively. The nucleation rate, J_n, can be expressed as

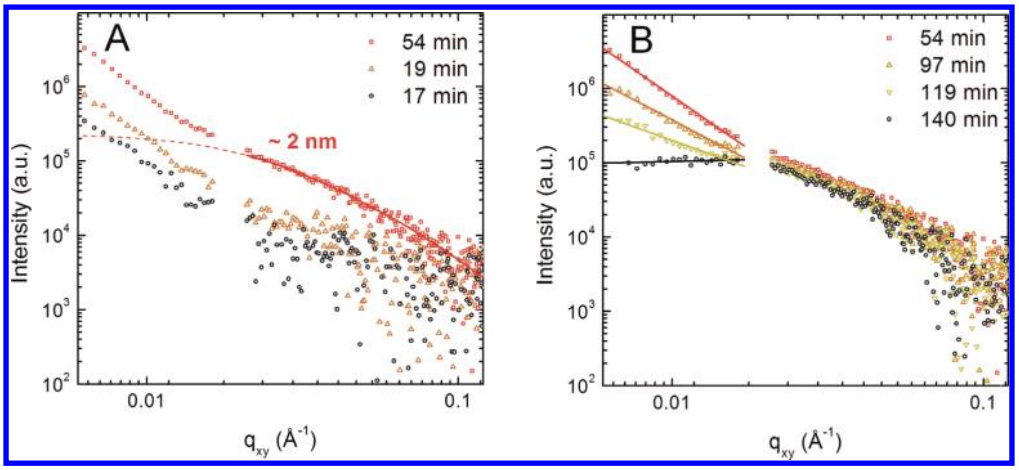

Figure 1. Horizontal cuts of the GISAXS intensity corresponding to experiment S3 (see Table 1A). (A) Particle scattering with an extended Guinier region is observed to develop with time. A fit to the data gives a very polydisperse population of particles with average particle size of ~2 nm. (B) After a given time, the slope of the particle scattering starts to decrease, concomitantly with a decrease of the negative slope of the signal at low q associated with a change in the aggregation state of the ~2 nm particles. The gaps in the data are due to a gap between different panels in the 2-dimensional detector.

dx.doi.org/10.1021/es3014826 | Environ. Sci. Technol. 2013, 47, 102−109

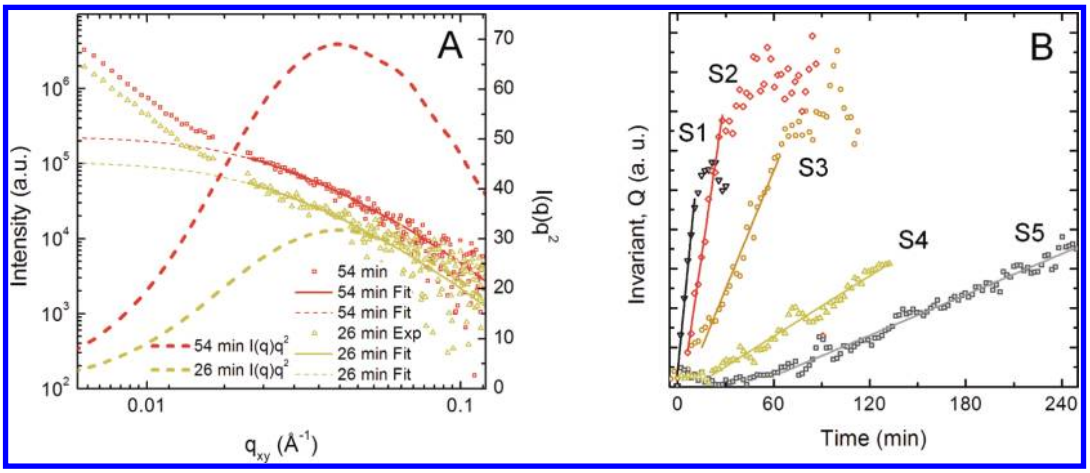

Figure 2. (A) Fits to the data at two different time points corresponding to experiment S3. The Lorentz-corrected SAXS scattering function is plotted (thick dashed lines). The invariant Q, proportional to the total mass nucleated, is equivalent to the area subtended underneath the thick dashed lines. (B) Evolution of the invariant with time at different supersaturations, and linear fits to the data.

$$J_n = A\exp\left(-\frac{\Delta g_n}{k_B T}\right) = A\exp\left(-\frac{16\pi {v_m}^2 \alpha'^3}{3{k_B}^3 T^3 \sigma^2}\right) \quad (3)$$

where Δg_n is the free energy change associated with the nucleation of the new phase, v_m is the molar volume of the nucleated phase divided by the Avogadro number, k_B is the Boltzmann constant, T is the temperature, and A is a kinetic factor containing another exponential law and an activation energy related to the kinetic pathways involved in nucleation. Homogeneous nucleation processes are governed by interfacial free energies between the nucleated particles and the solution ($\alpha' = \alpha_{lc}$). In the case of heterogeneous nucleation processes, three different interfacial free energies come into play: the liquid–nucleating crystal interfacial free energy α_{lc}, the liquid–substrate interfacial free energy α_{ls} and the substrate–crystal interfacial free energy α_{cs}. A fourth parameter, the contact angle θ between the nucleated particle and the substrate, is also an independent variable in the definition of the effective interfacial free energy for a spherical cap particle α' (see eq S2 in the Supporting Information (SI)). Assuming a hemispherical particle ($\theta = 90°$), eq S2 in the SI reduces to[29]

$$\alpha' = \frac{\alpha_{lc}}{2^{1/3}}\left(1 - \frac{\alpha_{ls} - \alpha_{sc}}{2\alpha_{lc}}\right) \quad (4)$$

A complete characterization of the thermodynamics of heterogeneous nucleation is thus possible if the nucleation rate is determined experimentally, and the other parameters in eqs 3 and 4 are known. The GISAXS experiments described here have been designed to obtain the rate of heterogeneous nucleation of $CaCO_3$ on quartz from the fits of a simple polydisperse model of spherical particles to the data. Experiments have been performed in a flow-through system to keep σ constant. Nucleation rates at different σ values have been obtained by making use of the SAXS invariant, Q:[27]

$$Q = (1/2\pi^2)\int q^2 I(q)dq \quad (5)$$

■ RESULTS AND DISCUSSION

Horizontal cuts to the normalized scattering data from one representative time-resolved experiment are shown in Figure 1. A power law behavior is observed at early stages of the nucleation experiment, with no particle scattering visible. With time, an increase in the scattered intensity is observed at intermediate q values. This is associated with the formation of $CaCO_3$ particles on the quartz substrate. A fit to the data in this region using a spherical model and a log-normal distribution to represent the polydispersity yields a mean particle size (radius) of ~2 nm (see SI), with typical standard deviation values of ~0.09 nm. At longer times (~54 min for the example shown in Figure 1), a different process is observed, with the intensity from the particle scattering decreasing at the same time as the exponent of the power law behavior observed at low q is decreased from −2.9 to ~0. This trend, which has been observed in all the experiments, can be interpreted based on previous studies as a change in the aggregation state of particulates formed by the ~2 nm elementary particles.[30,31] The apparent formation of a peak at around q = 0.03 Å^{-1} at long times (Figure 1b, 140 min) indicates that interparticle correlations between the elementary $CaCO_3$ particles are present, which could be modeled using an interparticle structure factor.[30,32,33] It is worth noting that all the curves also show power law behavior at very low q that could be associated with larger size entities. We hypothesize that the observed aggregation process is the basis of an aggregation-based growth model in which large crystals with sizes not probed within the q-range of these experiments are formed with time. Confirmation of the existence of these larger crystals is given by the observation that at long times (t > 100 min for the experiment shown in Figure 1) the scattered intensity around the beam center increases and shows reflections typical of faceted crystalline particles (see Figure S2 in the SI). A more complex analysis using different levels of mass fractal aggregate models could have been applied if the data quality would have been better. The curve at 54 min in Figure 1A could be decomposed into two different linear regions with different mass fractal exponents, indicating that the aggregate structure could have several levels of complexity.[33,34] However, the low statistics of our data sets—due to the low contrast between the nucleated particle and the surrounding solution and to the thick beam path through water (1 cm)—prevent any complex analysis of the data. Thus, we have restricted our data analysis to the time points during which the intensity is increasing (time points from 0 to 54 min in Figure 1A). In the data analysis we have interpreted the scattered curves using the simplest

dx.doi.org/10.1021/es3014826 | Environ. Sci. Technol. 2013, 47, 102–109

approach, with a single particle scattering region at medium and high q range plus a power law to describe the intensity at low q. No attempt has been made to model the structure factor observed in the curves at long times. More experiments at lower q ranges are needed to understand the size evolution of the aggregates, which is beyond the scope of this manuscript.

Analyzing the development of particle scattering at the initial stages of the experiments (such as those presented in Figure 1A) under different supersaturation conditions allows us to obtain thermodynamic information of the $CaCO_3$−quartz system. The observed increase of the intensity at early stages of the experiment is associated with the formation of ∼2 nm primary particles. Interestingly, the size of these primary particles remains constant during these initial stages (see fits of the data at different time points in the SI). According to eqs 1 and 2, three factors affect the total level of scattered intensity, namely the contrast ($\Delta\rho$), the square of the particle volume (V) and the number of particles (n). The fact that no change is observed in the size of the particles during these initial stages of the experiments, and under the assumption that the nature of the $CaCO_3$ polymorph that is being formed remains unchanged, we can make the assumption that V and $\Delta\rho$ are constant. The increase in the intensity can thus be solely ascribed to the nucleation of primary particles. The X-ray scattering invariant represents the integrated scattering intensity and is proportional to the total volume of particles irradiated by X-rays multiplied by the mean square of the electron density differences between the particles and water.[27]

Plots of the so-called Lorentz-corrected GISAXS intensity ($f(q) = I(q)\cdot q^2$) for two representative curves from the same experiment shown in Figure 1 are shown in Figure 2A. These curves have been calculated from the fitted function to the experimental data, which allows extrapolating the data at high q values and obtaining a converged value for the invariant at each time point. The invariant is equivalent to the subtended area underneath the Lorentz-corrected GISAXS intensity curves. Plots with the time-evolution of the invariant for a set of experiments at different solution supersaturation values are shown in Figure 2B, together with linear fits to the data. Following the observation that the size of the primary particles is constant throughout the early stages of the experiment, the slope of each of these curves is then equivalent to the rate of heterogeneous nucleation of $CaCO_3$ on quartz. The resulting nucleation rates are presented in Table 1A, and their natural logarithm are plotted against $1/\sigma^2$ in Figure 3. A linear regression of this plot yields a value for the slope that can be interpreted in terms of an interfacial free energy α' by using eq 3. From this, the value of the crystal−substrate interfacial free energy α_{cs} can be obtained using eq 4. However, some further hypotheses are required to make the calculations: (a) In order to obtain a value for the interfacial free energy α', the nucleated polymorph should be identified, so that the correct value for the molar volume (v_m) can be used in eq 3. Unfortunately, no information about the nature of the polymorph is available from the GISAXS experiment. In the absence of the information needed to ascertain the nature of the ∼2 nm nucleated particles, we decided to interpret the result by making two different assumptions about the nature of the polymorph, assuming the molar volumes for calcite[35] and for amorphous calcium carbonate (ACC) (see SI). (b) Also, values for the interfacial free energies between the water and the nucleated crystals are needed (α_{lc}). To our knowledge this value has only been reported for the surface of calcite (10−4),

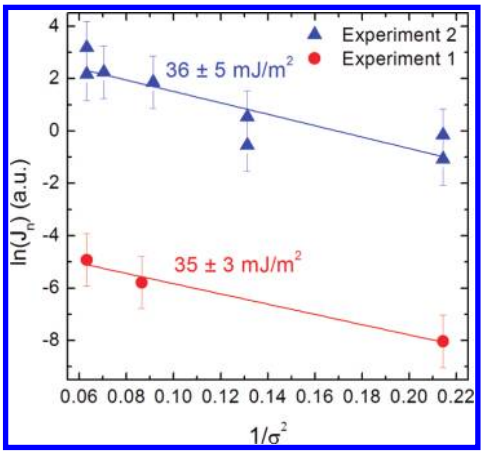

Figure 3. Plots of the measured nucleation rates against the inverse of the squared supersaturation. The obtained slope is proportional to the effective interfacial free energy α'. The data from two different synchrotron runs are shown.

showing a large variability: values of $\alpha_{water\text{-}calcite}$ range from 83 to 170 mJ/m^2.[36−39] In view of this variability, we decided to adopt a mean value of $\alpha_{water\text{-}calcite}$ = 120 mJ/m^2. For ACC, $\alpha_{water\text{-}ACC}$ is not known. However, given the highly hydrated state of ACC, we can make the reasonable assumption that this value must be lower than the minimum value that has been reported for calcite. Therefore, the value of $\alpha_{water\text{-}ACC}$ was assumed to be 50 mJ/m^2. Our choice of calcite and ACC as the possible nucleating polymorphs is founded also on the fact that their α_{lc} values are probably placed at the ends of the range of values expected for aragonite and vaterite (whose α_{lc} values are unknown). The same holds for the values of $v_{m,}$ with the exception of aragonite, that is denser than calcite. However, aragonite is rarely observed as the first polymorph nucleated (in the absence of Mg^{2+}), being ACC and vaterite the typically observed polymorphs in Ostwald ripening processes. It is also worth noting that, based on the ACC solubility constant reported by Brecevic and Nielsen,[25] ACC is not expected to nucleate under the conditions used in our experiments. However, the current ongoing debate in the literature about the possibility that $CaCO_3$ prenucleation clusters—formed in undersaturated conditions with respect to calcite—act as precursors for the nucleation of other polymorphs has prompted us to consider the possibility that ACC is the nucleating phase.[40,41] (c) The third parameter of relevance is related to the shape of the nucleated particles. This is important because the contact angle of the nuclei with the substrate has an influence on the exact form of equation (S4).[14,42] However, the small size of the nucleated particles observed in the GISAXS experiments lead us to question whether it is reasonable to define a shape for these small molecular clusters. For the sake of simplicity, and in the absence of further experimental evidence (e.g., high resolution microscopy data at the early stages of nucleation), a hemispherical shape (θ = 90°) has been assumed (results using other θ values are presented in the SI). (d) Values for the liquid−substrate interfacial free energies α_{ls} are needed if eq 4 is to be solved completely. Surprisingly, there are few reports for these values in the literature, and they are quite different from each other. Parks[43] reported a value $\alpha_{water\text{-}quartz}$ = 360 ± 30 mJ/m^2, which differs greatly from the $\alpha_{water\text{-}quartz}$ = 120 mJ/m^2 reported by Rimstidt and Cole[44] and is smaller than the value $\alpha_{water\text{-}quartz}$ = 416 mJ/m^2 published by Iler.[45] In a subsequent study, Mizele et al.[46] reported a value for

dx.doi.org/10.1021/es3014826 | Environ. Sci. Technol. 2013, 47, 102−109

the water−amorphous silica interface of $\alpha_{water\text{-}am\text{-}silica}$ = 340 mJ/m^2, which compares well with the value for quartz reported by Parks.[43] Amorphous silica and quartz surfaces differ on the different proportions of silanol groups on their surface and on the higher presence of defects present on the surface of amorphous silica, which might tend to increase the value of the liquid−substrate interfacial free energy.[46] However, a large variation in the value of α_{ls} is not expected.[43,46] According to this, we used the $\alpha_{water\text{-}quartz}$ = 360 ± 30 mJ/m^2 value reported by Parks,[41] which agrees well with the Mizele et al.[44] and is an intermediate value between all the reported values for the water−quartz interface.

The values for the different interfacial free energies calculated following the aforementioned assumptions are presented in Table 1B. If calcite is assumed to be the nucleated polymorph, a value of α' = 36 mJ/m^2 is obtained. Instead, if the ∼2 nm particles are assumed to be ACC nanoparticles, the interfacial free energy governing heterogeneous nucleation decreases to a value of α' = 27 mJ/m^2. These two values compare well with a previously measured value of α' = 31.1 mJ/m^2 reported by Lioliou et al. using a similar plot of the $CaCO_3$ precipitation rate (measured using bulk concentrations of $CaCO_3$) versus the inverse of the supersaturation.[17] However, these authors used a powder of quartz grains that was added to a supersaturated $CaCO_3$ solution after homogeneous nucleation had been initiated. It is thus possible that the agreement between both α' values is purely coincidental. In this sense, the fact that we are probing heterogeneous nucleation directly at the water-mineral interface, using a nanoscale in situ technique, and averaging over a large area of the substrate (the fingerprint of the X-ray beam on the substrate is about 1000 mm^2) makes our approach unique.

The fact that both α' values are smaller than $\alpha_{water\text{-}calcite}$ = 120 mJ/m^2 implies that the thermodynamic driving force for heterogeneous nucleation of $CaCO_3$ on quartz is higher than for homogeneous nucleation. A comparison between the height of the molar free energy barriers for nucleation (Δg_n) for both processes gives a ratio $\Delta g_{n\text{-}hete}/\Delta g_{n\text{-}homo} \times 100 = 2.5\%$ for calcite and an estimated ratio of $\Delta g_{n\text{-}hete}/\Delta g_{n\text{-}homo} \times 100 = 15\%$ lower if ACC is the nucleated polymorph. This implies that, if nucleation is an activated process, heterogeneous nucleation will be more significant over homogeneous nucleation, given that kinetically limiting factors for both processes are unimportant. An interesting point worth underlining here is that heterogeneous nucleation processes dominate even though obtained interfacial free energies $\alpha_{calcite/ACC\text{-}quartz}$ have relatively high values if compared, for instance, with values of $\alpha_{water\text{-}calcite/ACC}$. The effect of the substrate is represented in eq 4 by the factor in the parentheses. If this factor is equal to 1, the interfacial free energy governing the nucleation barrier would be equal to α_{lc}, which would be the case for a process of homogeneous nucleation. If the term in the parentheses is larger than 1, then heterogeneous nucleation is not favored thermodynamically and homogeneous nucleation will dominate. For heterogeneous nucleation to be favorable from a thermodynamic point of view, the term in the parentheses has to be lower than 1. This condition is fulfilled as long as the interfacial free energy between the solution and the substrate is larger than the interfacial free energy between the nucleated crystal and the substrate ($\alpha_{ls} > \alpha_{cs}$). This can be interpreted as a "competition" between the solution and the nucleating crystal for the substrate. Substrate hydrophilicity/hydrophobicity (associated with α_{ls}) and lattice mismatch (associated with α_{cs}) are thus the key parameters controlling heterogeneous nucleation.

Environmental Implications for Geologic Carbon Sequestration. The results presented here suggest that quartz is a favorable substrate for the nucleation of $CaCO_3$ under ambient conditions of pressure and temperature. This is a factor that can be readily included in pore scale reactive transport models of $CaCO_3$ nucleation where mineralogy is dominated by quartz, such as sandstone reservoirs. If the value for the interfacial energy obtained remains unchanged at the high temperatures and pressures present in geologic CO_2 storage reservoirs, and given that the nucleation process is not governed by kinetic factors, this could have significant implications in the prediction of sandstone reservoir permeability/porosity relationships, which are dependent on the spatial distribution of the precipitates.[47] Of course, conditions in geologic reservoirs will be different, with temperature and pressures typically higher than those of the critical point for CO_2 (31.1 °C and 7.38 MPa).[48,49] High temperature will be an additional driver for nucleation given the inverse solubility of carbonate minerals. However, the effect of both high pressure and temperature over the relative driving forces for heterogeneous (i.e., interfacial free energies) and homogeneous nucleation has not yet been obtained.

It is well-known that the wettability of mineral surfaces decreases after being in contact with $scCO_2$, becoming thus more hydrophobic.[50−52] According to the previous discussion, this change will affect the thermodynamics of nucleation by changing the difference between the term α_{ls}, which will increase (this term is minimum in the case of an ideal water/water interface), and the term α_{cs}, whose evolution is uncertain. The magnitude of α_{cs} is mostly controlled by the lattice mismatch between substrate and the nucleating crystal at the interface.[53] Given that the change in wettability will be mostly due to changes in the hydroxylation state of the substrate, as suggested by Chiquet et al.,[51] or to the capping of silanol groups with CO_2, as suggested by Dickson et al.,[52] and assuming no change in the lattice mismatch, one could hypothesize that the change in α_{cs} will be small. Under this assumption, the contact with $scCO_2$ is expected to increase the thermodynamic driving force for heterogeneous nucleation by providing an increase of α_{ls} that would lower the effective interfacial free energy for nucleation, α'. One interesting point is that the sole examination of α_{cs} cannot provide enough information of the likelihood of heterogeneous nucleation processes, which would be favored as long as α_{cs} is lower than α_{ls}. This fact highlights the need for an accurate determination of liquid−substrate interfacial free energies. The lack of this information not only affects our ability to predict accurately thermodynamic controls on nucleation processes, but it also prevents us from determining accurately the thermodynamics factors controlling dissolution processes. As reported by Lasaga and Blum,[54] the critical free-energy ΔG_c for the formation of an edge pit in a mineral surface depends directly on the value of the liquid−substrate interfacial free energy. This fact emphasizes the urgent need for more research in this direction.

Another important finding provided by a close examination of eq 4 is the fact that high salinity causes an increase of α_{ls}, as has been shown by Mizele et al.[46] in amorphous silica surfaces in contact with a 1 M NaCl solution. This is of special relevance for mineral carbonation in reservoir rocks due to the fact that some of the targeted sedimentary reservoirs are connected with salt domes, which requires that the pore-space water have high

dx.doi.org/10.1021/es3014826 | Environ. Sci. Technol. 2013, 47, 102−109

salinities up to 2 M NaCl.[21,55,56] A similar effect could be observed in depleted oil reservoirs proposed as potential CO_2 sequestration sites. The elevated concentrations of hydrophobic organic molecules forming coatings of mineral surfaces could increase the value of α_{ls}, as indicated by Butkus and Grasso[57] in organic-water interfaces. Salinity and organic coatings could therefore act as potential drivers for enhanced heterogeneous nucleation, from a purely thermodynamic point of view. Further investigations are needed to ascertain the effects that high ionic strength or the presence of organic molecules might have on the nucleation kinetics of metal carbonates.

■ ASSOCIATED CONTENT

Supporting Information

Descriptions of the Experimental details, five figures (homogeneous vs heterogeneous nucleation, 2-dimensional image from long reaction times, experimental setup, representative GISAXS patterns from different experiments and α_{sc} interfacial free energy values obtained using a spherical model with variable contact angle) and one table. This material is available free of charge via the Internet at http://pubs.acs.org.

■ AUTHOR INFORMATION

Corresponding Author

*Phone: 510-495-2224 (G.A.W.), 314-935-4539 (Y.-S.J.). Fax: 510-486-5686 (G.A.W.), 314-935-7211 (Y.-S.J.). E-mail: GAWaychunas@lbl.gov (G.A.W.), ysjun@seas.wustl.edu (Y.-S.J.).

Present Address

[||]ISTerre, CNRS and University of Grenoble I, Grenoble, 38041, France

Notes

The authors declare no competing financial interest.

■ ACKNOWLEDGMENTS

We gratefully acknowledge James J. DeYoreo for numerous discussions and for his insightful comments and suggestions, as well as the constructive comments from four reviewers. Also, Jessica Ray (WUStL), Xiaobing Zuo, Janae DeBartolo and Sonke Seifert (APS, ANL) are thanked for their help during GISAXS data collection. A.F.-M. thanks Giuseppe Saldi, Damien Daval and the 'Amorphous Reading Group' for enjoyable discussions about this and other subjects over the last two years. This material is based upon work supported as part of the Center for Nanoscale Control of Geologic CO_2, an Energy Frontier Research Center funded by the U.S. Department of Energy, Office of Science, Office of Basic Energy Sciences under Award Number DE-AC02-05CH11231. Use of the Advanced Photon Source, an Office of Science User Facility operated for the U.S. Department of Energy Office of Science by Argonne National Laboratory, was supported by the U.S. DOE under Contract No. DE-AC02-06CH11357.

■ REFERENCES

(1) Pacala, S.; Socolow, R. Stabilization wedges: Solving the climate problem for the next 50 years with current technologies. *Science* **2004**, *305*, 968−972.

(2) Lackner, K. S. A guide to CO_2 sequestration. *Science* **2003**, *300*, 1677−1678.

(3) Matter, J. M.; Kelemen, P. B. Permanent storage of carbon dioxide in geological reservoirs by mineral carbonation. *Nature Geoscience* **2009**, *2*, 837−841.

(4) Riding, R. Microbial carbonates: The geological record of calcified bacterial-algal mats and biofilms. *Sedimentology* **2000**, *47*, 179−214.

(5) Dean, W. E. J. Determination of carbonate and organic matter in calcareous sediments and sedimentary rocks by loss on ignition: Comparison with other methods. *J. Sed. Petrol.* **1974**, *44*, 242−248.

(6) Tegethoff, F. W.; Rohleder, J.; Kroker, E. *Calcium Carbonate: From the Cretaceous Period into the 21st Century*; Birkhäuser Basel, 2002; p 351.

(7) Benson, S. M.; Cole, D. R. CO_2 sequestration in deep sedimentary formations. *Elements* **2008**, *4*, 325−331.

(8) Prigiobbe, V.; Costa, G.; Baciocchi, R.; Hänchen, M.; Mazzotti, M. The effect of CO_2 and salinity on olivine dissolution kinetics at 120°C. *Chem. Eng. Sci.* **2009**, *64*, 3510−3515.

(9) Daval, D.; Martinez, I.; Corvisier, J.; Findling, N.; Goffe, B.; Guyot, F. Carbonation of Ca-bearing silicates, the case of wollastonite: Experimental investigations and kinetic modeling. *Chem. Geol.* **2009**, *265*, 63−78.

(10) Guyot, F.; Daval, D.; Dupraz, S.; Martinez, I.; Menez, B.; Sissmann, O. CO_2 geological storage: The environmental mineralogy perspective. *C. R. Geosci.* **2011**, *343*, 246−259.

(11) Béarat, H.; McKelvy, M. J.; Chizmeshya, A. V. G.; Gormley, D.; Nunez, R.; Carpenter, R. W.; Squires, K.; Wolf, G. H. Carbon sequestration via aqueous olivine mineral carbonation: Role of passivating layer formation. *Environ. Sci. Technol.* **2006**, *40*, 4802−4808.

(12) Saldi, G. D.; Schott, J.; Pokrovsky, O. S.; Gautier, Q.; Oelkers, E. H. An experimental study of magnesite precipitation rates at neutral to alkaline conditions and 100−200°C as a function of pH, aqueous solution composition and chemical affinity. *Geochim. Cosmochim. Acta* **2012**, *83*, 93−109.

(13) Giammar, D.; Bruantr, R.; Peters, C. Forsterite dissolution and magnesite precipitation at conditions relevant for deep saline aquifer storage and sequestration of carbon dioxide. *Chem. Geol.* **2005**, *217*, 257−276.

(14) DeYoreo, J. J.; Vekilov, P. G. Principles of crystal nucleation and growth. *Rev. Mineral. Geochem.* **2003**, *54*, 57−93.

(15) Lin, Y.; Singer, P. Effects of seed material and solution composition on calcite precipitation. *Geochim. Cosmochim. Acta* **2005**, *69*, 4495−4504.

(16) Kralj, D.; Vdovic, N. The influence of some naturally occurring minerals on the precipitation of calcium carbonate polymorphs. *Water Res.* **2000**, *34*, 179−184.

(17) Lioliou, M. G.; Paraskeva, C. A.; Koutsoukos, P. G.; Payatakes, A. C. Heterogeneous nucleation and growth of calcium carbonate on calcite and quartz. *J. Colloid Interface Sci.* **2007**, *308*, 421−428.

(18) Di Tommaso, D.; de Leeuw, N. H. Structure and dynamics of the hydrated magnesium ion and of the solvated magnesium carbonates: Insights from first principles simulations. *Phys. Chem. Chem. Phys.* **2010**, *12*, 894−901.

(19) Ostroverkhov, V.; Waychunas, G. A.; Shen, Y. R. Vibrational spectra of water at water/α-quartz (0001) interface. *Chem. Phys. Lett.* **2004**, *386*, 144−148.

(20) Churchill, H.; Teng, H.; Hazen, R. M. Correlation of pH-dependent surface interaction forces to amino acid adsorption: Implications for the origin of life. *Am. Mineral.* **2004**, *89*, 1048−1055.

(21) Kharaka, Y.; Cole, D.; Thordsen, J.; Kakouros, E.; Nance, H. Gas−water−rock interactions in sedimentary basins: CO_2 sequestration in the Frio Formation, Texas, USA. *J. Geochem. Explor.* **2006**, *89*, 183−186.

(22) Jun, Y.-S.; Lee, B.; Waychunas, G. A. In situ observations of nanoparticle early development kinetics at mineral−water interfaces. *Environm. Sci. Technol.* **2010**, *44*, 8182−9.

(23) Hu, Y.; Lee, B.; Bell, C.; Jun, Y.-S. Environmentally abundant anions influence the nucleation, growth, ostwald ripening, and aggregation of hydrous Fe(III) oxides. *Langmuir* **2012**, *28*, 7737−7746.

(24) Charlton, S. R.; Macklin, C. L.; Parkhurst, D. L. *PHREEQCI—A Graphical User Interface for the Geochemical Computer Program*

PHREEQC; U.S. Geological Survey Water-Resources Investigations Report 97-4222, 1997; p. 9.
(25) Brecevic, L.; Nielsen, A.-E. Solubility of amorphous calcium carbonate. *J. Cryst. Growth* **1989**, *98*, 504−510.
(26) Renaud, G.; Revenant, C.; Barbier, A.; Noblet, M.; Ulrich, O.; Jupille, J.; Borensztein, Y.; Henry, C. R.; Deville, J.-paul; Scheurer, F.; Mane-mane, J.; Fruchart, O. Real-time monitoring of growing nanoparticles. *Science* **2003**, *300*, 1416−1419.
(27) Guinier, A. *X-Ray Diffraction in Crystals, Imperfect Crystals, and Amorphous Bodies*; Dover Publications Inc., 1994.
(28) Ilavsky, J.; Jemian, P. R. Irena: Tool suite for modeling and analysis of small-angle scattering. *J. Appl. Crystallogr.* **2009**, *42*, 347−353.
(29) Lasaga, A. C. *Kinetic theory in the Earth sciences*; Princeton University Press, 1998; p 811.
(30) Tatou, M.; Genix, A.-caroline; Imaz, A.; Forcada, J.; Schweins, R.; Grillo, I.; Oberdisse, J. Reinforcement and polymer mobility in silica-latex nanocomposites with controlled aggregation. *Macromolecules* **2011**, *44*, 9029−9039.
(31) Wijnen, P. W. J. G.; Beelen, T. P. M.; Rummens, K. P. J.; Saeijs, H. C. P. L.; Santen, R. A. V. Silica gel from water glass: A SAXS study of the formation and ageing of fractal aggregates. *J. Appl. Crystallogr.* **1991**, *24*, 759−764.
(32) Oberdisse, J.; Hine, P.; Pyckhout-Hintzen, W. Structure of interacting aggregates of silica nanoparticles in a polymer matrix: Small-angle scattering and reverse Monte Carlo simulations. *Soft Matter* **2007**, *3*, 476.
(33) Beaucage, G. Small-angle scattering from polymeric mass fractals of arbitrary mass-fractal dimension. *J. Appl. Crystallogr.* **1996**, *29*, 134−146.
(34) Beaucage, G.; Rane, S.; Sukumaran, S.; Satkowski, M. M.; Schechtman, L. A.; Doi, Y. Persistence length of isotactic poly(hydroxy butyrate). *Macromolecules* **1997**, *30*, 4158−4162.
(35) Markgraf, S. A.; Reeder, S. A. High-temperature structure refinements of calcite and magnesite. *Am. Mineral.* **1985**, *70*, 590−600.
(36) Duffy, D. M.; Harding, J. H. Simulation of organic monolayers as templates for the nucleation of calcite crystals. *Langmuir* **2004**, *20*, 7630−6.
(37) Bennema, P.; Söhnell, O. Interfacial surface tension for crystallization and precipitation from aqueous solutions *P. bennema*. *J. Cryst. Growth* **1990**, *102*, 547−556.
(38) Söhnel, O.; Mullin, J. W. A method for the determination of precipitation induction periods. *J. Cryst. Growth* **1978**, *44*, 377−382.
(39) Liu, X. Y.; Lim, S. W. Templating and supersaturation-driven anti-templating: Principles of biomineral architecture. *J. Am. Chem. Soc.* **2003**, *125*, 888−895.
(40) Gebauer, D.; Volkel, A.; Colfen, H. Stable prenucleation calcium carbonate clusters. *Science* **2008**, *322*, 1819−1822.
(41) Gebauer, D.; Cölfen, H. Prenucleation clusters and non-classical nucleation. *Nano Today* **2011**, *6*, 564−584.
(42) Travaille, A. M.; Steijven, E. G. A.; Meekes, H.; van Kempen, H. Thermodynamics of epitaxial calcite nucleation on self-assembled monolayers. *J. Phys. Chem. B* **2005**, *109*, 5618−26.
(43) Parks, G. Surface and interfacial free energies of quartz. *J. Geophys. Res.* **1984**, *89*, 3997−4008.
(44) Rimstidt, J.; Cole, D. Geothermal mineralization; I, The mechanism of formation of the Beowawe, Nevada, siliceous sinter deposit. *Am. J. Sci.* **1983**, *283*, 861−875.
(45) Iler, R. K. *The Chemistry of Silica: Solubility, Polymerization, Colloid and Surface Properties and Biochemistry of Silica*; Wiley, 1979; p 365.
(46) Mizele, J.; Dandurand, J.; Schott, J. Determination of the surface energy of amorphous silica from solubility measurements in micropores. *Surf. Sci.* **1985**, *V*, 830−837.
(47) Armstrong, R.; Ajo-Franklin, J. Investigating biomineralization using synchrotron based X-ray computed microtomography. *Geophys. Res. Lett.* **2011**, *38*, L08406.
(48) Shao, H. B.; Ray, J. R.; Jun, Y. S. Dissolution and precipitation of clay minerals under geologic CO_2 sequestration conditions: CO_2-brine-phlogopite interactions. *Environ. Sci. Technol.* **2010**, *44*, 5999−6005.
(49) Hu, Y.; Ray, J. R.; Jun, Y.-S. Biotite-brine interactions under acidic hydrothermal conditions: Fibrous Illite, goethite, and kaolinite formation and biotite surface cracking. *Environ. Sci. Technol.* **2011**, *45*, 6175−80.
(50) Espinoza, D. N.; Santamarina, J. C. Water−CO_2−mineral systems: Interfacial tension, contact angle, and diffusion—Implications to CO_2 geological storage. *Water Resour. Res.* **2010**, *46*, 1−10.
(51) Chiquet, P.; Broseta, D.; Thibeau, S. Wettability alteration of caprock minerals by carbon dioxide. *Geofluids* **2007**, *7*, 112−122.
(52) Dickson, J. L.; Gupta, G.; Horozov, T. S.; Binks, B. P.; Johnston, K. P. Wetting phenomena at the CO_2/water/glass interface. *Langmuir* **2006**, *22*, 2161−2170.
(53) Jun, Y.-S.; Kendall, T. A.; Martin, S. T.; Friend, C. M.; Vlassak, J. J. Heteroepitaxial nucleation and oriented growth of manganese oxide islands on carbonate minerals under aqueous conditions. *Environ. Sci. Technol.* **2005**, *39*, 1239−1249.
(54) Lasaga, A. C.; Blum, A. E. Surface chemistry, etch pits and mineral-water reactions. *Geochim. Cosmochim. Acta* **1986**, *50*, 2363−2379.
(55) Shao, H.; Ray, J. R.; Jun, Y.-S. Effects of organic ligands on supercritical CO_2-induced phlogopite dissolution and secondary mineral formation. *Chem. Geol.* **2011**, *290*, 121−132.
(56) Shao, H.; Ray, J. R.; Jun, Y. -shin Effects of salinity and the extent of water on supercritical CO_2 - induced phlogopite dissolution and secondary mineral formation. *Environ. Sci. Technol.* **2011**, 1737−1743.
(57) Butkus, M.; Grasso, D. Impact of aqueous electrolytes on interfacial energy. *J. Colloid Interface Sci.* **1998**, *181*, 172−181.

NOTE ADDED AFTER ASAP PUBLICATION

The values in Table 1b were incorrect, and the Supporting Information was modified in the version of this paper published July 18, 2012. The correct version published July 19, 2012.